Lab on a Chip

PAPER

Cite this: *Lab Chip*, 2017, **17**, 3431

Reproducible fiber optofluidic laser for disposable and array applications†

Chaoyang Gong,[a] Yuan Gong, *[ab] Qiushu Chen,[b] Yun-Jiang Rao,[a] Gang-Ding Peng[c] and Xudong Fan *[b]

Received 7th July 2017,
Accepted 23rd August 2017

DOI: 10.1039/c7lc00708f

rsc.li/loc

Disposable sensors are widely used in biomedical detection due to their inherent safety, ease of use and low cost. An optofluidic laser is a sensitive bioassay platform; however, demonstrating its fabrication cheaply and reproducibly enough for disposable use has been challenging. Here, we report a low-cost, reproducible fiber optofluidic laser (FOFL) using a microstructured optical fiber (MOF). The MOF not only supports the whispering gallery modes for lasing but also serves as a microfluidic channel for sampling the liquid gain medium *via* capillary force. Because of the precise control of its geometry ($\delta < 0.4\%$) during the fiber-drawing process, good reproducibility in laser intensity ($\delta = 6.5\%$) was demonstrated by changing 10 sections of the MOF. The strong coupling between the in-fiber resonator and gain medium enables a low threshold of 3.2 μJ mm^{-2}. The angular dependence of the laser emission was observed experimentally and analyzed with numerical simulations. An array of the FOFLs was also demonstrated. This technology has great potential for low-cost bioassay applications.

Introduction

Optofluidic lasers[1–7] can distinguish very small changes in both the structure[8,9] and concentration[10] of biomolecules. To date, only reusable optofluidic laser sensors (OFLSs) have been demonstrated, although disposable sensors[11–15] are preferred in biomedical assays. The main challenge in developing disposable OFLSs is how to cost-effectively mass-produce micro-resonators with good batch-to-batch reproducibility in geometry and thus optical quality.

Fabry–Perot resonators consisting of highly reflective mirrors[10,16,17] are usually costly and difficult to mass-assemble with good reproducibility. Stand-alone droplets[18–20] or microspheres[2,21] have been employed as micro-ring resonators for lasing; however, it is not convenient to handle such single micro-cavities as sensors. Thin-walled capillaries can support whispering gallery modes (WGMs) in their cross-sections.[1,3,4] The laboratory heating-and-drawing method is capable of fabricating a capillary with a wall thickness down to <1 μm, but this method is not feasible for mass production. Commercial thin-walled capillaries were tested in our experiments, but no lasing was observed (see Fig. S1† for details). Although a thick-walled capillary is also usable as an optofluidic laser, lasing can be observed only when the gain medium is a solution with a refractive index higher than that of the wall ($n > 1.45$) and with optical feedback from the total internal reflection on the inner wall;[22] this is inconsistent with the refractive index of samples ($n < 1.4$) in bio-applications.

The cylindrical microcavity of common optical fibers (COFs) can serve as a micro-ring resonator for an optofluidic laser.[9,23–25] The COF can be mass-produced (~50 km in length) at a low cost (~0.01 USD per meter) with a fiber draw tower. Most importantly, its diameter is highly reproducible, with a variation of ~0.56% (125 ± 0.7 μm, SMF-28e, Corning) on the kilometer scale, making it a resonator candidate for a disposable optofluidic laser. However, the solid core of the COF makes it inconvenient for liquid sampling.

In this paper, we report a fiber optofluidic laser (FOFL) based on a microstructured optical fiber (MOF). The MOF has two holes in its cross-section and can draw the liquid gain medium by capillary action. High-order whispering gallery modes, confirmed by numerical simulations, provide the optical feedback. Lasing was observed with a low threshold of 3.2 μJ mm^{-2}. Similar to the COF, the MOF can be mass-produced with low cost and high reproducibility in diameter. The FOFL output was repeatable when different sections of the MOF were tested, enabling its disposable use. An FOFL array was

[a] *Key Laboratory of Optical Fiber Sensing and Communications (Ministry of Education of China), University of Electronic Science and Technology of China, No. 2006, Xiyuan Ave., Chengdu, 611731 China. E-mail: ygong@uestc.edu.cn*
[b] *Department of Biomedical Engineering, University of Michigan, 1101 Beal Ave, Ann Arbor, MI, 48109, USA. E-mail: xsfan@umich.edu*
[c] *School of Electrical Engineering and Telecommunications, University of New South Wales, Sydney, NSW 2052, Australia*

† Electronic supplementary information (ESI) available. See DOI: 10.1039/c7lc00708f

also demonstrated, showing the potential of multiplexed detection.

Simulation

To reveal the optical feedback mechanism in our MOFs, numerical simulation was performed based on finite element analysis (FEA). First, a spot source was placed at location A (x = 57.5 μm, y = 0 μm) to excite the resonance modes (Fig. 1a). The wavelength of the spot source was set at approximately 556 nm. The simulation was conducted in the dashed box, exploiting the MOF's symmetric geometry. The intensity distribution in Fig. 1a was obtained by mirroring twice (see Fig. S2† for details). Bright polygonal beams can be clearly observed; they correspond to the high-order WGMs. The yellow arrows represent the output beams from the MOF, indicating four maximum emission peaks at 45°, 135°, 225° and 315°.

The intensity distribution on the x-axis of Fig. 1a is shown in Fig. 1b, demonstrating multi-mode characteristics in the range of 57.5 μm to 75 μm. The penetration depth, d_e, of the evanescent wave into the hole is defined as the distance at which the light intensity decays to 1/e of the maximum. d_e was determined to be approximately 230 nm (inset of Fig. 1b).

The source was then placed at different locations away from A within the hole, and no resonances of light were obtained, as presented in Fig. S3.† The simulation results indicated that only the emission from gain molecules near A can couple strongly with WGMs, leading to strong enhancement of light in the MOF.

Experimental

A schematic of the experimental setup for the fiber optofluidic laser is shown in Fig. 2 (see Fig. S4† for details). The gain medium, 1 mM Rhodamine 6G (R6G) in ethanol, was drawn into the MOF by capillary action. A 532 nm pulsed laser (Continuum, 5 ns pulse width, 20 Hz repetition rate) was focused by a cylindrical lens, which forms a narrow strip (0.5 mm × 5 mm) and is incident perpendicularly on the MOF. Due to the optical resonance of the high-order WGM in the cross-section (Fig. 1a), lateral laser emission can be observed. A long-pass edge filter with a cut-on wavelength of 550 nm was used to filter out the pump laser. The laser emission was collected by a lens and sent to a spectrometer (Andor, SR500IA).

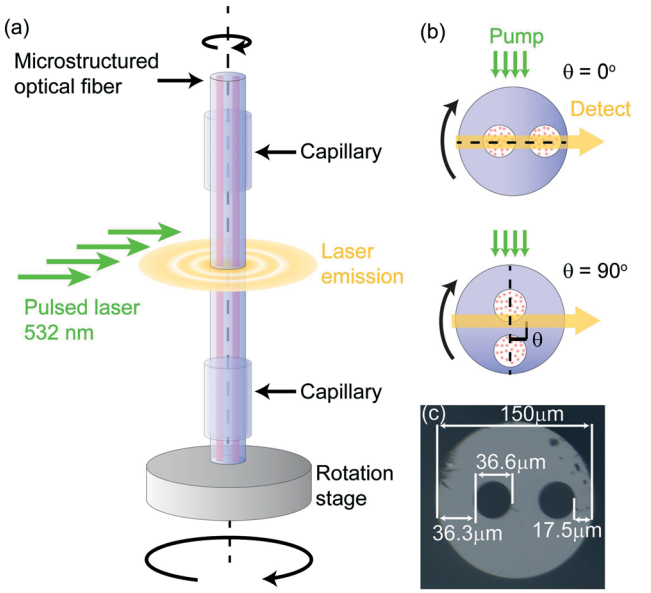

Fig. 2 (a) Schematic diagram of the experimental setup for the fiber optofluidic laser and (b) the top view of its cross-section. (c) A microscopy image of the cross-section of the MOF. The MOF was held by two sections of capillaries with inner diameters of ~200 μm and could be rotated with a resolution of 1°. The axes of the pump and the detection were fixed at 90°. The MOF was rotated with an angle of θ (Fig. 2b and Video S1†) to investigate the angular dependence of the laser emission.

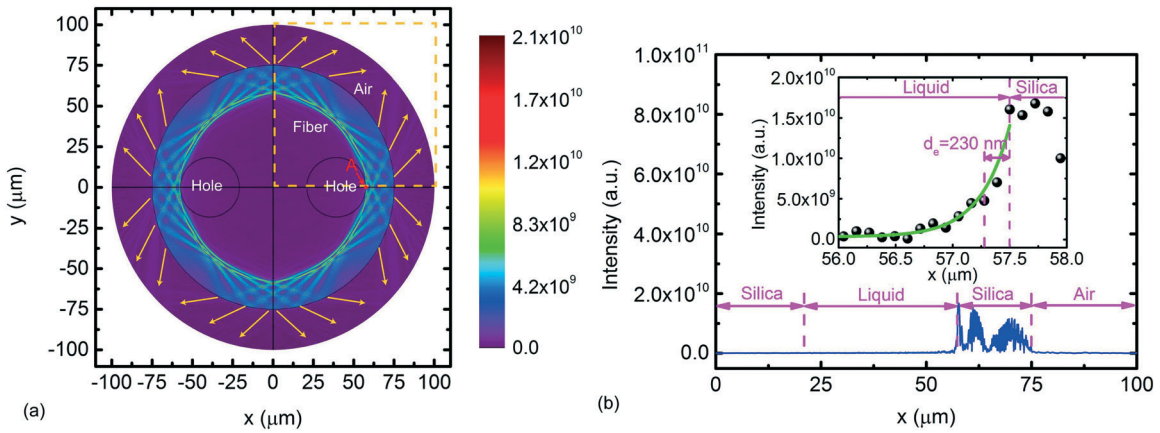

Fig. 1 Numerical simulations. (a) Intensity distribution in the cross-section of the MOF. (b) Light intensity on the x-axis. Inset: the enlargement of the curve. The black circles denote the simulation data, and the green curve is an exponential fit. In the model, the diameters of the fiber and the inner holes were set at 150.0 μm and 36.6 μm, respectively. The thinnest part of the MOF is 17.5 μm. The refractive indices of the silica fiber and the dye-filled holes were set at 1.46 and 1.36, respectively.

The MOF was fabricated by drilling holes in a preform and drawing using a commercial fiber draw tower to a long length (kilometers) with good uniformity. This fiber could thus be produced at low cost (<1 USD per meter, details for cost calculation are given in the ESI†) with good consistency (<0.4% deviation) required for disposable sensors. The diameters of the MOF and holes were 150 μm and 36.6 μm, respectively (Fig. 2c). After removing the coating layer, the MOF was cleaved into sections with lengths of 3 cm and immersed in sulfuric acid (98%) overnight. It was then washed for 5 min in an ultrasonic bath of deionized (DI) water 3 times. The MOF was further cleaned in plasma (140 W) for 10 min, making it clean and highly hydrophilic; the liquid gain medium could be drawn easily into the holes by capillary action. Hundreds of MOFs could be batch-processed simultaneously.

Results and discussion

First, lateral lasing from the MOF was demonstrated, and the spectral and threshold characteristics of the FOFL were investigated. We fixed θ at 125° where the maximum laser emission was observed. A photo of the FOFL is shown in Fig. S5.† The laser spectra were recorded under various pump energy densities (Fig. 3a). The free spectral range (FSR) was 0.47 nm. By using FSR = $\lambda_1\lambda_2/(2\pi r n_{\mathrm{eff}})$, where λ_1 and λ_2 are the respective wavelengths of adjacent longitudinal modes and n_{eff} is the effective refractive index, the diameter of the resonance micro-ring, $2r$, was determined to be 143.5 μm (Fig. 2c). The result confirms that the laser feedback is provided by the high-order WGM (see Fig. 1). The integrated intensity was calculated using $P(\theta=125^\circ)=\int I(\lambda,\theta)\mathrm{d}\lambda$ and is shown as a function of pump density in Fig. 3b, indicating a laser threshold of 3.2 μJ mm^{-2}, which is comparable to those of capillary-based optofluidic lasers[26] and better than that based on a fiber-in-capillary structure.[24]

According to the threshold, we estimated the Q factor of the ring resonator. At the lasing threshold, the gain should be equal to the loss which can be written as

$$\zeta\Delta N\sigma_{\mathrm{e}}(\lambda)=\zeta\sigma_{\mathrm{a}}(\lambda)N+\frac{2\pi n}{\lambda Q}$$

Here, ζ is the fraction of mode energy coupling with the gain medium, ΔN is the concentration of dye molecules in the excited state, σ_{e} is the emission cross-section at the lasing wavelength and σ_{a} is the dye absorption cross-section at the lasing wavelength. n is the refractive index of the gain medium and Q is the quality factor of the cavity mode. Thus, we can derive that

$$\gamma_{\mathrm{th}}=\frac{\Delta N}{N}=\frac{\sigma_{\mathrm{a}}(\lambda)}{\sigma_{\mathrm{e}}(\lambda)}\left(1+\frac{2\pi n}{\lambda\zeta NQ\sigma_{\mathrm{a}}(\lambda)}\right)$$

On the other hand, at the excitation intensity just above the threshold, the population inversion can be written as

$$\gamma=\frac{w_{\mathrm{p}}\tau_{\mathrm{rad}}}{1+w_{\mathrm{p}}\tau_{\mathrm{rad}}}$$

which is derived from a standard four-level system. τ_{rad} is the radiation lifetime of the dye (3.7 ns for R6G). Given the threshold excitation intensity of 3.2 μJ mm^{-2}, γ can be calculated to be 0.0654. By letting γ_{th} = 0.0654, the effective Q-factor ζQ is estimated to be around 400, given that the extinction coefficient of R6G at 558 nm is 6.5 × 10^3 cm^{-1} M^{-1}, the emission cross-section is 1 × 10^{-14} cm^2 and the concentration is 1 mM. With ζ calculated to be 1% in our simulation, the passive Q factor of the WGMs that support lasing is estimated to be around 4 × 10^4.

Second, the angular dependence of the laser emission was investigated. The rotation angle, θ, was adjusted from 0° to 360° with a step of 5°, and the spectra were recorded. The intensity was spectrally integrated and is shown as a function of θ in Fig. 4a and b. The distribution shows four peaks at 50°, 125°, 225° and 295°, and the corresponding laser spectra are shown in Fig. 4c. The asymmetry in the peak intensity and angular location was partially induced by the

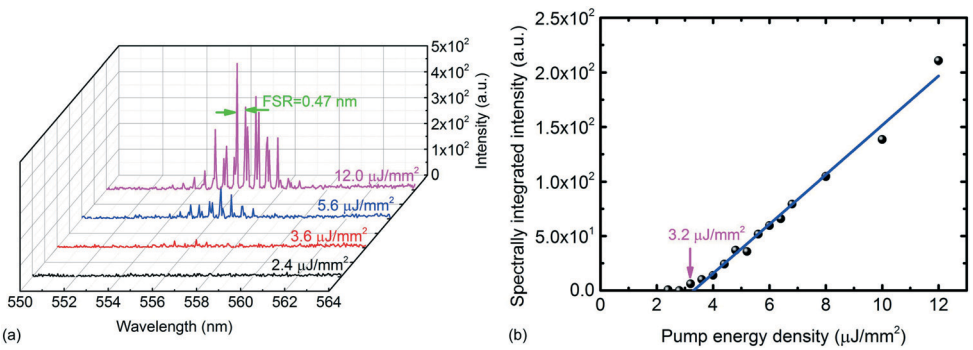

Fig. 3 Lasing characteristics of the optofluidic laser using a microstructured optical fiber. (a) Laser spectra. The pump energy density varied from 2.4 μJ mm^{-2} to 12 μJ mm^{-2}. The MOF was filled with 1 mM R6G in ethanol. (b) The spectrally integrated intensity as a function of pump energy density. The intensity is spectrally integrated between 552 nm and 561 nm. The threshold of the fiber optofluidic laser is approximately 3.2 μJ mm^{-2}. The rotation angle of the MOF was θ = 125°.

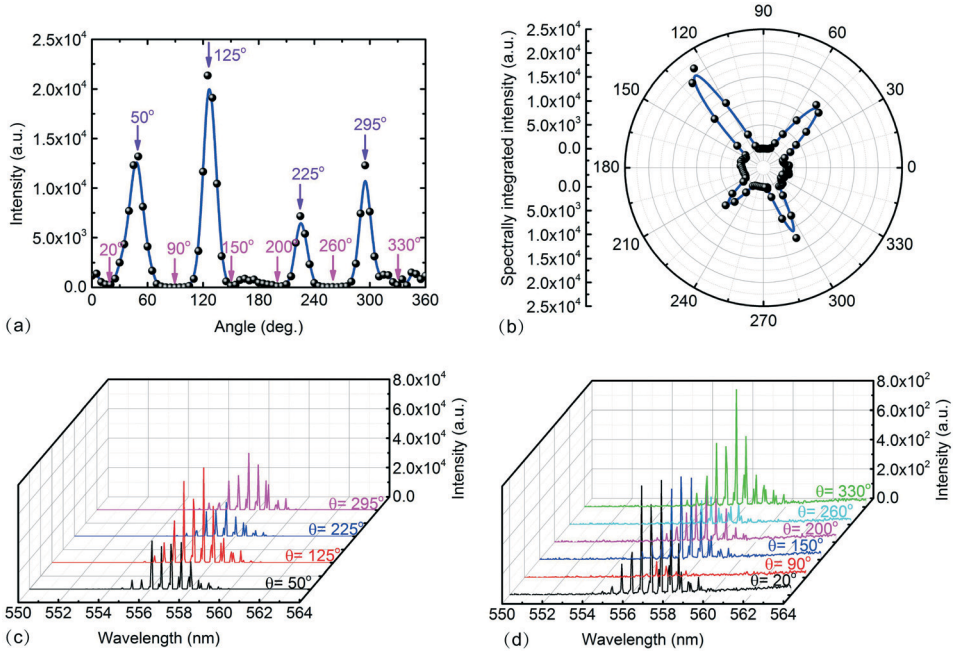

Fig. 4 Angular dependence of the lateral laser emission. Spectrally integrated intensity *versus* the rotation angle in (a) rectangular and (b) polar coordinate systems. The spectra of strong and weak laser emissions at different angles are shown in (c) and (d), respectively. The pump energy density was fixed at 120 μJ mm^{-2}.

imperfection of the symmetry of the MOF, as well as the non-uniformity of pump density when the MOF was rotated. The laser can also be observed at minima in Fig. 4a at angles of 20°, 90°, 150°, 200°, 260° and 330°, with the spectra given in Fig. 4d. The results are also shown in Video S1.†

Third, the repeatability of the FOFL was evaluated. The laser emission was measured 10 times from the same MOF. For each angle, the spectrally integrated intensity was statistically averaged to be $\overline{P(\theta)} = \frac{1}{10}\sum\int I_i(\lambda,\theta)\mathrm{d}\lambda$. The results are

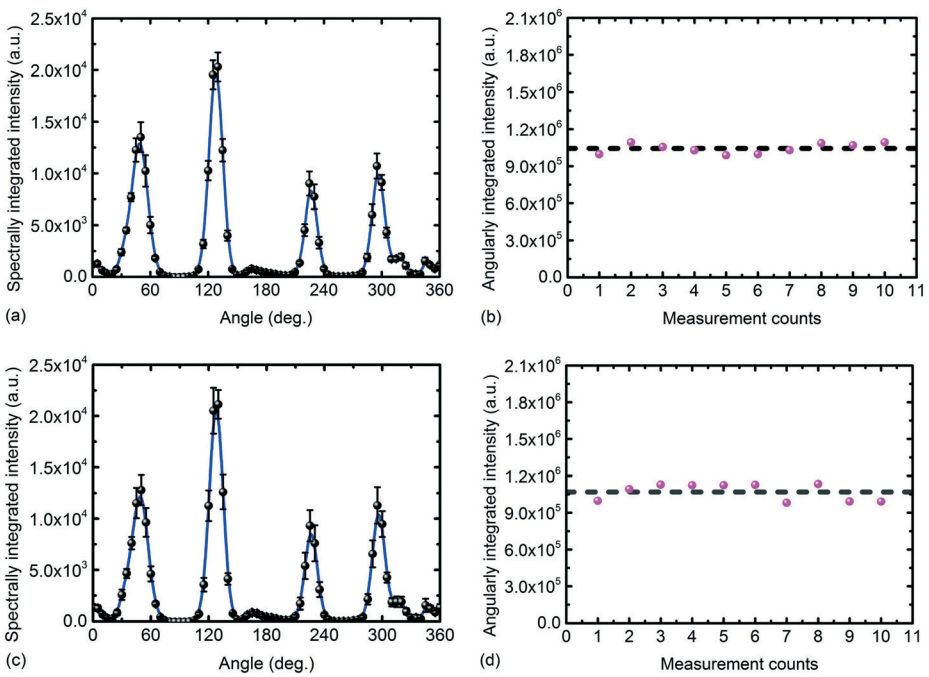

Fig. 5 Repeatability of the FOFL output. Angular dependence of the laser emission for 10 tests using (a) the same and (c) different sections of MOFs. The corresponding angularly integrated intensities are shown in (b) and (d), respectively. The dashed line denotes the mean value of 10 tests. The pump energy density was 120 μJ mm^{-2}.

shown in Fig. 5a; the error bars indicate the small coefficients of variation (CVs). The intensity was then integrated over both wavelength and angle to obtain the total laser output for each test: $P_i = \int_0^{360°} \int I_i(\lambda,\theta) \mathrm{d}\lambda \mathrm{d}\theta$ (i = 1, 2, 3,…, 10) (dots in Fig. 5b). The statistical deviation of 10 tests, δ_1 = ±3.9%, resulted from the fluctuation of the pump energy density, which was influenced by the instability of the MOF's lateral position and the fluctuation of the pump energy.

The feasibility of disposable FOFLs was then demonstrated by measuring the laser output from 10 different sections of the MOF (10 cm apart). The results are shown in Fig. 5c and d. The deviation of 10 tests, δ_2 = ±6.5%, is slightly higher than that using the same MOF but is still small, especially for bioassays with a large dynamic range spanning 4–6 orders of magnitude.[10,27–29] Therefore, the reproducibility of this kind of FOFL is sufficient for single-use bioassays. Further, the cost of one 3 cm section of the MOF is very low (<0.03 USD), suitable for disposable use.

Finally, an array of FOFLs was demonstrated (Fig. 6). All MOFs were oriented in the same manner with the longer-distance hole up and fixed using UV glue. A motorized translational stage was used to scan the FOFLs one by one in the *x*-axis direction. The emission spectra were recorded each time the translational stage stepped 0.1 mm. Fig. 6c shows the integrated intensity as a function of the lateral position. Four FOFL channels were clearly identified. The deviation of the flat-top of each channel was approximately 7.1%; it varied randomly and was mainly from the pump instability. The deviation between different channels was approximately 13.1% and arose from the imperfect orientation of each MOF.

Compared with the optofluidic laser array based on the high-finesse Fabry–Perot cavity,[30] the advantages of the MOF-based optofluidic laser array are as follows: (1) liquid sampling based on capillary action is easy and convenient. (2) The geometry of the fiber micro-cavity, and thus the volume of the liquid gain medium, can be accurately controlled. The microfluidic channel (holes) and the micro-resonator are highly integrated in the cross-section of the MOF. (3) The channels are separated spatially so that they do not influence each other in either sampling or optical feedback.

There are several ways to reduce the angular effect, thus reducing the variations from each FOFL channel. First, by calculating the angular integral of the intensity over 0–360°, variations among FOFL channels in the array can be reduced. Second, marking the direction of holes on fiber cladding during the fabrication process might be another way to improve the orientation accuracy for the FOFLs. As a prospect, angular multiplexing of FOFLs may be available, as there is a difference of two orders of magnitude between the maximum and the minimum intensity of the angle-dependent laser emission (Fig. 4c and d).

For future trials, we suggest the fabrication of hollow-core optical fibers (HOFs) with an ultrathin wall (1–2 μm

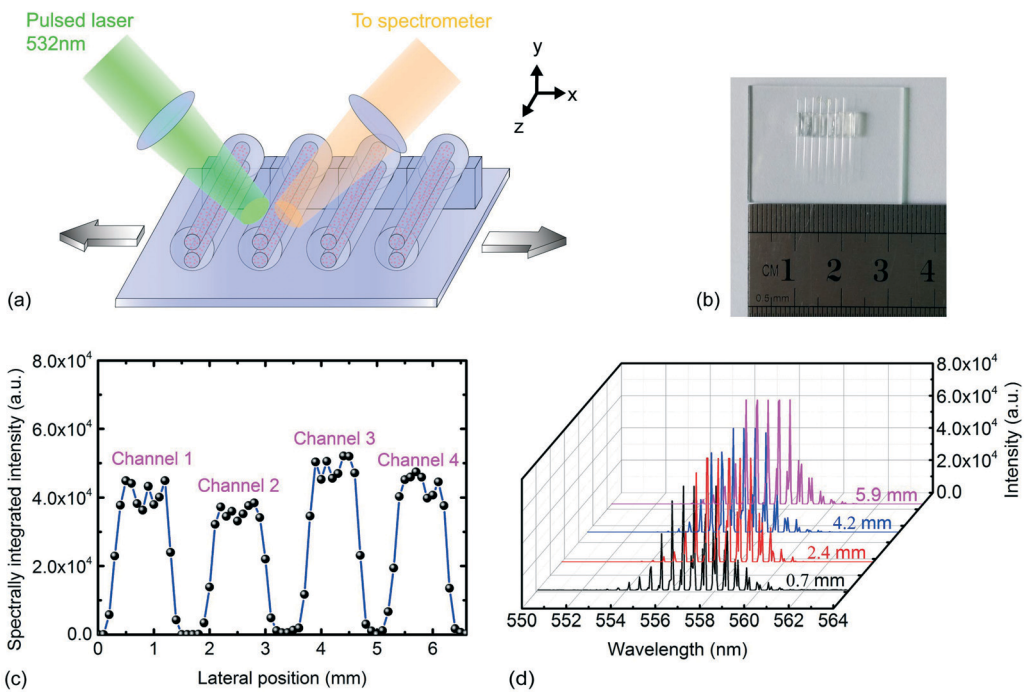

Fig. 6 (a) Schematic diagram and (b) photo of the FOFL array. Each MOF was fixed in a V-type groove with the two holes vertically oriented, and then the grooves were placed in parallel. Limited by the width of the groove, the spatial separation between two adjacent MOFs was approximately 1.5 mm. The crosstalk between adjacent laser channels was minimized by using a plano-convex lens (f = 100 mm), instead of the previously used cylindrical lens. The beam diameter of the pump laser on the MOF was approximately 0.65 mm, and consequently there was always only one channel being illuminated. (c) The spectrally integrated intensity as a function of the lateral pump position. The pump energy density was 180 μJ mm^{-2}. (d) The spectra from different channels of a FOFL.

thickness) using a fiber draw tower, which can further improve the FOFL with angular insensitivity and higher *Q*-factor, while maintaining its low cost and high reproducibility. However, ultrathin-walled HOFs are very fragile and easily break, and thus require careful handling.

Summary

We have demonstrated a reproducible fiber optofluidic laser using a micro-structured optical fiber. The MOF was used as both the laser cavity and the channel for liquid sampling. Laser emission from WGMs was observed with a low threshold. The angular dependence of laser emission was investigated experimentally. Thanks to the inherent ultra-small variations in MOF geometry, repeatable output of the FOFL was confirmed. Furthermore, a FOFL array was demonstrated. Our work provides reproducible, low-cost optofluidic lasers for potential disposable biomedical sensing applications.

Conflicts of interest

There are no conflicts of interest to declare.

Acknowledgements

We acknowledge financial support from the National Natural Science Foundation of China (61575039), the Fundamental Research Funds for the Central Universities (ZYGX2015J137), the 111 Project (B14039), and the National Science Foundation (DBI-1451127).

References

1 X. Fan and S. H. Yun, *Nat. Methods*, 2014, **11**, 141–147.
2 M. Humar and S. H. Yun, *Nat. Photonics*, 2015, **9**, 572–576.
3 H. Schmidt and A. R. Hawkins, *Nat. Photonics*, 2011, **5**, 598–604.
4 X. Fan and I. M. White, *Nat. Photonics*, 2011, **5**, 591–597.
5 C. Vannahme, F. Maier-Flaig, U. Lemmer and A. Kristensen, *Lab Chip*, 2013, **13**, 2675.
6 T. Wienhold, F. Breithaupt, C. Vannahme, M. B. Christiansen, W. Dorfler, A. Kristensen and T. Mappes, *Lab Chip*, 2012, **12**, 3734–3739.
7 C. Vannahme, M. B. Christiansen, T. Mappes and A. Kristensen, *Opt. Express*, 2010, **18**, 9280–9285.
8 Y. Sun and X. Fan, *Angew. Chem.*, 2012, **124**, 1262–1265.
9 W. Lee, Q. Chen, X. Fan and D. K. Yoon, *Lab Chip*, 2016, **16**, 4770–4776.
10 X. Wu, M. K. K. Oo, K. Reddy, Q. Chen, Y. Sun and X. Fan, *Nat. Commun.*, 2014, **5**, 3779.
11 G. Marrazza, I. Chianella and M. Mascini, *Biosens. Bioelectron.*, 1999, **14**, 43–51.
12 J. C. Chen, J. L. Shih, C. H. Liu, M. Y. Kuo and J. M. Zen, *Anal. Chem.*, 2006, **78**, 3752–3757.
13 U. Bog, F. Brinkmann, S. F. Wondimu, T. Wienhold, S. Kraemmer, C. Koos, H. Kalt, M. Hirtz, H. Fuchs, S. Koeber and T. Mappes, *Adv. Sci.*, 2015, **2**, 1500066.
14 M. Zourob, S. Mohr, B. J. T. Brown, P. R. Fielden, M. B. McDonnell and N. J. Goddard, *Biosens. Bioelectron.*, 2005, **21**, 293–302.
15 X. A. Ton, V. Acha, P. Bonomi, B. T. S. Bui and K. Haupt, *Biosens. Bioelectron.*, 2015, **64**, 359–366.
16 C. Gong, Y. Gong, M. K. K. Oo, Y. Wu, Y. Rao, X. Tan and X. Fan, *Biosens. Bioelectron.*, 2017, **96**, 351–357.
17 Y. Yang, A. Q. Liu, L. Lei, L. K. Chin, C. D. Ohl, Q. J. Wang and H. S. Yonn, *Lab Chip*, 2011, **11**, 3182–3187.
18 S. K. Y. Tang, Z. Li, A. R. Abate, J. J. Agresti, D. A. Weitz, D. Psaltis and G. M. Whitesides, *Lab Chip*, 2009, **9**, 2767–2771.
19 A. J. C. Kuehne, M. C. Gather, I. A. Eydelnant, S. H. Yun and D. A. Weitz, *Lab Chip*, 2011, **11**, 3716–3719.
20 A. Jonáš, M. Aas, Y. Karadag, S. Manioğlu, S. Anand, D. McGloin, H. Bayraktar and A. Kiraz, *Lab Chip*, 2014, **14**, 3093–3100.
21 S. Nizamoglu, M. C. Gather and S. H. Yun, *Adv. Mater.*, 2013, **25**, 5943–5947.
22 Y. Wang, K. S. Leck, V. D. Ta, R. Chen, V. Nalla, Y. Gao, T. He, H. V. Demir and H. Sun, *Adv. Mater.*, 2015, **27**, 169–175.
23 Q. Chen, M. Ritt, S. Sivaramakrishnan, Y. Sun and X. Fan, *Lab Chip*, 2014, **14**, 4590–4595.
24 Y. Zhang, W. Meng, H. Yang, Y. Chu and X. Pu, *Opt. Lett.*, 2015, **40**, 5101–5104.
25 H. J. Moon, Y. T. Chough and K. An, *Phys. Rev. Lett.*, 2000, **85**, 3161.
26 S. I. Shopova, H. Zhou, X. Fan and P. Zhang, *Appl. Phys. Lett.*, 2007, **90**, 221101.
27 Y. Park, B. Ryu, B. Oh, Y. Song, X. Liang and K. Kurabayashi, *ACS Nano*, 2017, **11**, 5697–5705.
28 J. J. Zhou, H. P. Huang, J. Xuan, J. R. Zhang and J. J. Zhu, *Biosens. Bioelectron.*, 2010, **26**, 834–840.
29 M. R. Monroe, G. G. Daaboul, A. Tuysuzoglu, C. A. Lopez, F. F. Little and M. S. Unlu, *Anal. Chem.*, 2013, **85**, 3698–3706.
30 W. Wang, C. Zhou, T. Zhang, J. Chen, S. Liu and X. Fan, *Lab Chip*, 2015, **15**, 3862–3869.

